# Temperature dependence of energy transfer mechanisms in Eu-doped GaN

Chang-Won Lee
*Department of Physics, Duke University, Durham, North Carolina 27708*

Henry O. Everitt[a)]
*Department of Physics, Duke University, Durham, North Carolina 27708*
*and U.S. Army Research Office, Research Triangle Park, North Carolina 27709*

D. S. Lee and A. J. Steckl
*Department of Electrical and Computer Engineering and Computer Science, University of Cincinnati, Cincinnati, Ohio 45221*

J. M. Zavada
*U.S. Army Research Office, Research Triangle Park, North Carolina 27709*

(Received 22 December 2003; accepted 19 March 2004)

The temperature dependent behavior of continuous-wave and time-resolved photoluminescence of Eu-doped GaN in the visible region is measured for both the $^5D_0 \rightarrow {}^7F_2$ and $^5D_0 \rightarrow {}^7F_3$ transitions. The radiative decay of these transitions, following pulsed laser excitation of the GaN host, is monitored by a grating spectrometer and photomultiplier tube detector system. In addition to these two radiative energy transfer pathways within $Eu^{3+}$, the data reveal two nonradiative energy transfer paths between $Eu^{3+}$ and the host GaN. Decay constants for the relaxation processes are extracted from the data using a numerically solved rate equation model. Although the dominant radiative relaxation processes decayed with a temperature insensitive decay constant of 166 $\mu$s, a prominent role for nonradiative transfer between $Eu^{3+}$ and impurities within the GaN host was deduced above 180 K. © *2004 American Institute of Physics.* [DOI: 10.1063/1.1738529]

## I. INTRODUCTION

Recently, rare-earth (RE) doped III–V semiconductors have been intensively studied for their potential use in integrated optoelectronic devices like visible (blue, green, red) and infrared luminescent devices.[1,2] Overcoming thermal and concentration-induced quenching and increasing the effective number of optically active RE ions in the host for enhanced efficiency will be necessary to make these devices useful. Er-doped Si and GaAs initially received much attention for their 1.54 $\mu$m IR emission, but wide band gap semiconductor hosts like GaN and ZnO have been shown to exhibit very efficient visible green emission (537 nm, 558 nm) as well.[3,4] This has stimulated the search for other RE dopants like $Eu^{3+}$ (red: 622 nm) and $Tm^{3+}$ (blue: 477 nm), in a variety of host materials to expand the spectrum in visible region.[5]

Rare-earth atoms in III–V semiconductors typically occupy cation substitutional sites with $C_{3v}$ symmetry, forming trivalent $RE^{3+}$ ions as long as they are not located near the surface.[6–9] The detected visible or infrared emissions from rare-earth ions arise from transitions between intra-$4f$ configuration levels that are partially filled. Electrons in these levels are strongly localized near the nucleus ($r<0.4$ Å) and shielded by the $5s^2$ and $5p^6$ orbitals. Therefore, they weakly participate in chemical bonding, and emission from intra-$4f$ shell transitions is nearly unaffected by the host type. As a further manifestation of host insensitivity, RE emission intensity varies much less with temperature than those of quantum well- or even quantum dot-based photon emitters, and the luminescence lines are much sharper ($Q \cong E/\Delta E \sim 200$). However, the RE ions are not completely immune to the host. Transitions between $4f$ levels of isolated $RE^{3+}$ ions are electric dipole forbidden transitions, so the host either relaxes the electric dipole selection rules through an additional crystal field perturbation (forced electric dipole transition) or allows non-negligible higher order transitions such as magnetic dipole or electric quadrupole transitions.[10–12] Quasiparticle formations, like excitonic polarons near a $RE^{3+}$ ion site, also affect transition probabilities between $4f$ states by relaxing forbidden selection rules.[13,14] The typical oscillator strength of allowed intra-$4f$ transitions is of order of $10^{-6}$, and luminescence decay times can be as slow as tens of milliseconds.

A combined and unified picture of the origin of luminescence and thermal quenching for various RE-doped semiconductors is emerging. Emission from the $4f$ transitions is enhanced when the nonradiative transition probabilities decrease and the population of RE ions in the excited states increases. Nonradiative energy transfer leakage pathways out of the $RE^{3+}$ ions, either by direct excitations or by delivering energy through the host material, clearly must be understood.

The study of combined spectral and temporal features of luminescence at different temperatures, excitation intensities, and energies can reveal the salient energy transfer mechanisms in RE-doped semiconductors. Here, we present temperature-dependent continuous-wave and time-resolved photoluminescence data for the visible emission in Eu-doped GaN. Simple rate equation models are developed to interpret and fit the data and to extract the decay constants.

a)Electronic mail: everitt@phy.duke.edu

 

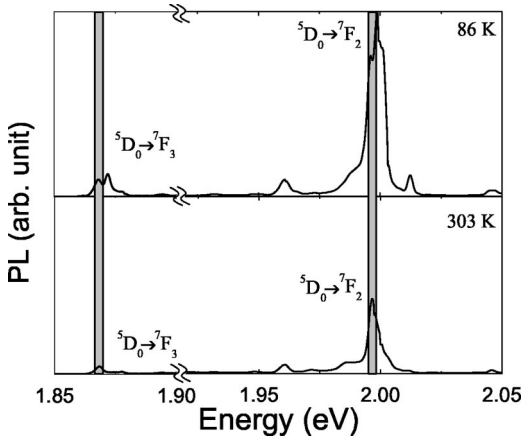


FIG. 1. CWPL spectra at 86 K and 303 K are shown. Two dominant emission lines from $Eu^{3+}$ ions at 1.99 eV (622.4 nm) for the $^5D_0 \rightarrow {}^7F_2$ transition and at 1.86 eV (665 nm) for the $^5D_0 \rightarrow {}^7F_3$ transition are clearly seen. The spectral windows encompassed by the subsequent TRPL data are indicated by the shaded regions.

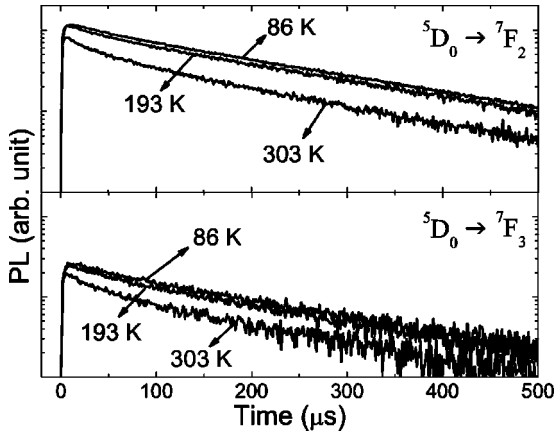


FIG. 2. TRPL signals for $^5D_0 \rightarrow {}^7F_2$ and $^5D_0 \rightarrow {}^7F_2$ transitions at three temperatures are shown. The logarithmic scale shows the deviations from the single exponential behavior in the first 50 $\mu$s.

## II. EXPERIMENT

The Eu-doped GaN sample was grown *in situ* on a Si(111) substrate by solid state molecular beam epitaxy (MBE). The spectra of RE-doped materials grown by this technique usually exhibit sharper and more homogeneous lines than that by other techniques like ion-implantation or gas source MBE.[15] The detailed sample preparation procedure is available elsewhere.[3] The estimated Eu concentration $\sim 10^{20}\,\mathrm{cm}^{-3}$ ($\sim$1 at. %) produces optimal red luminescence. Cross relaxation between $Eu^{3+}$ ions, which may suppress the luminescence efficiency, is expected to be negligible at this low concentration.

The continuous-wave photoluminescence (CWPL) excitation source was a HeCd laser operating at 3.815 eV (325.0 nm) and $\sim$2.5 W/cm$^2$. The pulsed excitation for the time-resolved photoluminescence (TRPL) was a frequency quadrupled signal of the superfluorescence from a wavelength-tunable optical parametric amplifier, pumped by a Ti:sapphire oscillator-seeded regenerative amplifier with a 1 kHz repetition rate. The temporal width of the 4.13 eV (300 nm) excitation pulse was less than 200 fs, and the excitation intensity was 1.18 $\mu$J/cm$^2$. The sample was mounted in a cryostat so the temperature could be varied between 86–303 K with 10 K steps and $\pm$1.5 K accuracy. Photoluminescence was collected by a lens and focused by a spherical mirror onto the input slit of a 0.75 m single grating monochrometer whose spectral resolution was adjusted to be 0.8 nm. The diffracted luminescence was detected by a thermo-electrically-cooled, 1000-V-biased Hamamatsu R928 photomultiplier tube which has a response time faster than 30 ns. Standard lock-in techniques were used to detect the CWPL signals. The detected TRPL signals were sampled and averaged by a digitizing oscilloscope with 1 GHz bandwidth.

## III. RESULTS

### A. Continuous wave photoluminescence

The 86 K and 303 K CWPL spectra of Eu-doped GaN are shown in Fig. 1. The sharp emission lines from the $Eu^{3+}$ do not shift significantly with temperature. The two most dominant $Eu^{3+}$ emission lines are associated with the $^5D_0 \rightarrow {}^7F_2$ transition (1.992 eV) and the $^5D_0 \rightarrow {}^7F_3$ transition (1.864 eV).[16–18] The $^5D_0 \rightarrow {}^7F_2$ transition in the $Eu^{3+}$ ion is an electric dipole type transition, but $^5D_0 \rightarrow {}^7F_3$ transition arises from non-negligible total angular momentum mixing.[12] The measured ratio of the spectrally integrated CWPL intensities approximates the ratio of the spontaneous emission probabilities of the $^5D_0 \rightarrow {}^7F_2$ transition to the $^5D_0 \rightarrow {}^7F_3$ transition. The measured value of 10.0 is very close to the reported value (9.95) in Eu-doped $YAlO_3$.[12]

$Eu^{3+}$ ions typically occupy substitutional sites with perfect $C_{3v}$ symmetry. With such placement, the $^5D_0 \rightarrow {}^7F_2$ transition is predicted to consist of three peaks due to crystal field splitting.[19] This triplet is observed in the low temperature, high resolution CWPL data. Furthermore, the $^5D_0 \rightarrow {}^7F_0$ transition (2.13 eV or 582 nm), which may only be activated by $Eu^{3+}$ at interstitial sites with lower symmetry than $C_{3v}$, was not detected.[19] In the case of the $^5D_0 \rightarrow {}^7F_3$ transition at 1.864 eV,[16,6,15] which is forbidden even when both crystal field splitting and $J-J$ mixing are considered,[10–12] a doublet is observed.

Negligible temperature dependent shifts ($<$0.1 nm) were detected from both the $^5D_0 \rightarrow {}^7F_2$ and $^5D_0 \rightarrow {}^7F_3$ transitions, but in both transitions only the lowest energy peak persists to 303 K. Moreover, the spectrally integrated 86 K emissions were quenched at 303 K by 5.0 and 3.6 times, respectively, indicating an important role for nonradiative recombination.

### B. Time-resolved photoluminescence

The temporal evolution of luminescence decay was measured for the $^5D_0 \rightarrow {}^7F_2$ and $^5D_0 \rightarrow {}^7F_3$ transitions for more than 23 temperatures between 86 K and 303 K (Fig. 2). The spectral window for TRPL is set to 4.9 meV and 4.5 meV, respectively, to cover the entire low energy-split peak of each transition (shaded regions in Fig. 1). The detected initial rise time is approximately 10 $\mu$s for all temperatures. The decay time is approximately 200 $\mu$s; however, the signal increasingly deviates from single exponential decay with increasing temperature.

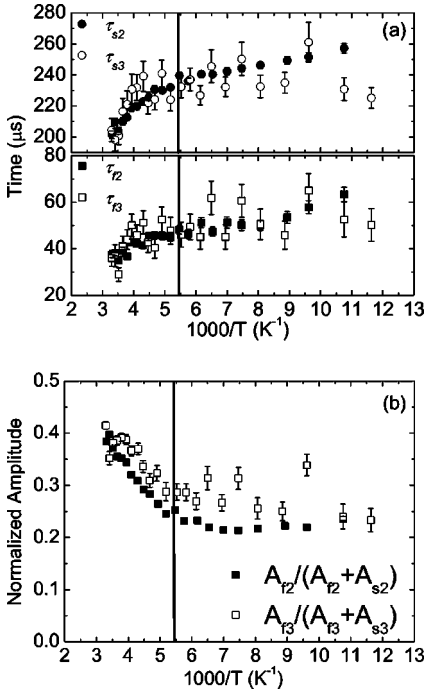


FIG. 3. (a) Biexponential fit results for the fast (squares) and slow (circles) decay times versus temperature of the $^5D_0 \rightarrow {}^7F_2$ (solid) and $^5D_0 \rightarrow {}^7F_3$ (open) transitions. (b) Biexponential fit results for the normalized amplitude versus temperature of the $^5D_0 \rightarrow {}^7F_2$ (solid) and $^5D_0 \rightarrow {}^7F_3$ (open) transition. Both indicate a clear change in temperature dependence at 180 K (1000/180 K=5.5).

Indeed, the decaying signal can be well fit by the phenomenological biexponential formula

$$I(t) = A_{fi} \exp\left(-\frac{t}{\tau_{fi}}\right) + A_{si} \exp\left(-\frac{t}{\tau_{si}}\right), \tag{1}$$

where $i=2,3$ for $^5D_0 \rightarrow {}^7F_2$ and $^5D_0 \rightarrow {}^7F_3$, respectively. The temperature dependencies of the fitted decay times ($\tau_{fi}$ and $\tau_{si}$ for the faster and slower component, respectively) and the normalized amplitudes ($A_{fi}/(A_{fi}+A_{si})$) of the $^5D_0 \rightarrow {}^7F_2$ and $^5D_0 \rightarrow {}^7F_3$ transitions are shown in Figs. 3(a) and 3(b), respectively. To within experimental uncertainty, the component decay times for both transitions are the same at a given temperature. Both decay times increasingly accelerate with increasing temperature. The slower decay time, $\tau_{si}$, is likely associated with transitions involving both temperature-insensitive radiative decay and temperature sensitive nonradiative decay mechanisms. This observation is consistent with prior measurements of decay lifetimes in other RE-doped semiconductor systems.[14,15] The faster decay time, $\tau_{fi}$, reflects the action of additional nonradiative relaxation mechanisms that depopulate the $^5D_0$ state. The normalized amplitude of the ''fast'' component is a nearly constant 25% at temperatures below 180 K (16 meV), then it increases to approximately 40% of the signal by 300 K. This suggests a temperature-dependent, nonradiative decay with a 16 meV activation energy for the underlying mechanism.

In an attempt to characterize these decay features, the microscopic analysis introduced by Inokuti and Hirayama,[20–22]

$$I(t) \cong I(0) \exp\left(\frac{t}{\tau_0} - A\left(\frac{t}{\tau_0}\right)^{3/s} \Gamma\left(1-\frac{3}{s}\right)\right), \tag{2}$$

was used to fit the data, where $\Gamma(x)$ is the gamma function. This analysis assumes the dominant nonradiative relaxation pathway arises from cross relaxation between $Eu^{3+}$ ions. The second term in the exponential arises from the assumption that $RE^{3+}$ ions act as donors, where $A$ contains the phenomenological donor–acceptor cross-relaxation rate that is inversely proportional to the $s$th power of the average distance between two ions. If $s$ is 6, 8, and 10, then the type of the cross-relaxation is dipole–dipole, dipole–quadrupole, and quadrupole–quadrupole, respectively.[22]

Although acceptable fits to the data were obtained using (2), the derived value for the parameter $s$ is an unphysical $s<3$. This supports the earlier assertion that the $Eu^{3+}$ ion concentration in this material is not high enough for any significant multipole–multipole interactions between $Eu^{3+}$ ions. Other nonradiative relaxation mechanisms are at work, and another model that includes these dominant mechanisms must be developed.

### C. Time-integrated photoluminescence

Another insight into the underlying dynamics is obtained by comparing the temperature-dependent correlation between $\tau_{si}$ and the time-integrated photoluminescence (TIPL) intensities of both transitions (Fig. 4). The intensity of the photon emission is proportional to the transition probability, so the fact that the low temperature TIPL intensities and $\tau_{si}$ have the same temperature dependence suggests that radiative recombination is the dominant low temperature relaxation process. Above 180 K, both the TIPL intensity and $\tau_{si}$ drop, indicating that much of the decrease in emission intensity may be attributed to the accelerating decay constant $\tau_{si}$. However, the TIPL intensity drops more steeply with temperature than $\tau_{si}$, suggesting the onset of another competitive relaxation pathway with a corresponding activation energy of 16 meV. This is the second indication of this nonradiative process first observed in the increasing prominence of the faster biexponential TRPL decay feature above 180 K.

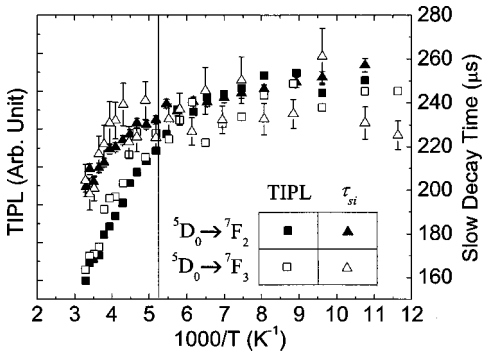


FIG. 4. A combined plot of the temperature-dependent time-integrated photoluminescence (TIPL) and $\tau_{si}$ from the biexponential fits of both transitions. TIPL values begin to deviate from the $\tau_{si}$ values above 180 K, suggesting the onset of a nonradiative energy transfer process.

## IV. SIMULATION

In order to characterize these relaxation processes, a more complex phenomenological energy transfer model was developed, and the ability of the physically-motivated model to reproduce the TRPL data was used to identify the most important processes. The decay constants from various radiative and nonradiative energy transfer processes were obtained by the fitting the model to the entire TRPL trace, including the initial rising edge, for both transitions at a given temperature.

In constructing this model, a number of assumptions were made. First, the energy transfer pathway that excites the $^5D_0$ state of the $Eu^{3+}$ ions starts with excitation of the GaN host material because the absorption cross section of $Eu^{3+}$ ions at 4.13 eV is negligible compared to that of band-to-band transition of the GaN host.[23] Therefore, the action of the laser can be simulated as a sudden rise in the exciton density of the host. Second, because the temporal resolution of the detection system was approximately 30 ns, faster processes could be ignored and a quasiequilibrium existed among many states. For example, because the radiative and nonradiative recombination of band–band and free excitons in the host is so fast ($<1$ ns),[24] the recombination process in the host concludes quickly and was not modeled. This implies that the host GaN conduction band is largely depopulated during the time scale of the TRPL measurements, although long-lived ''bound excitons at'' impurities, traps, and ''Eu'' dopants in the host may remain. Likewise, it is not necessary to describe the details of the individual intramanifold relaxation processes within the $^5D_J$ and $^7F_J$ manifolds.[25] The energy transfer pathways from the host through the $^5D_J$ manifold to the $^5D_0$ state of the $Eu^{3+}$ can simply be represented by a single effective rate constant ($\tau_{HE}$). Third, thermal re-excitation of any $^7F_J$ state to any $^5D_J$ state can be ignored because the energy difference is large and the process is too slow at the temperatures used in this experiment. Finally, relaxation away from $^7F_2$ and $^7F_3$ into other, lower energy manifolds occurs much more quickly than they are filled, so decay into these states effectively removes carriers from the monitored energy transfer pathways. It was not assumed the $^5D_0 \rightarrow {}^7F_2$ and $^5D_0 \rightarrow {}^7F_3$ transitions were identical in their dynamics. Both transitions were fitted simultaneously, and the resulting rates represented the most self-consistent solution for both transitions.

From this, a series of increasingly complex rate equation models was constructed in order to analyze the data [Fig. 5(a)]. Various energy transfer processes that transfer this electronic excitation between the GaN host, the $Eu^{3+}$ dopants, and the salient impurities and traps were considered. The output of the models is the predicted population difference of the $^5D_0 \rightarrow {}^7F_2$ and $^5D_0 \rightarrow {}^7F_3$ transitions, plotted as a function of time and compared to the TRPL data for the corresponding temperature. Both the $^5D_0 \rightarrow {}^7F_2$ and $^5D_0 \rightarrow {}^7F_3$ TRPL data were modeled and fit simultaneously, and the obtained rates self-consistently characterize the processes that depopulate or repopulate $^5D_0$.

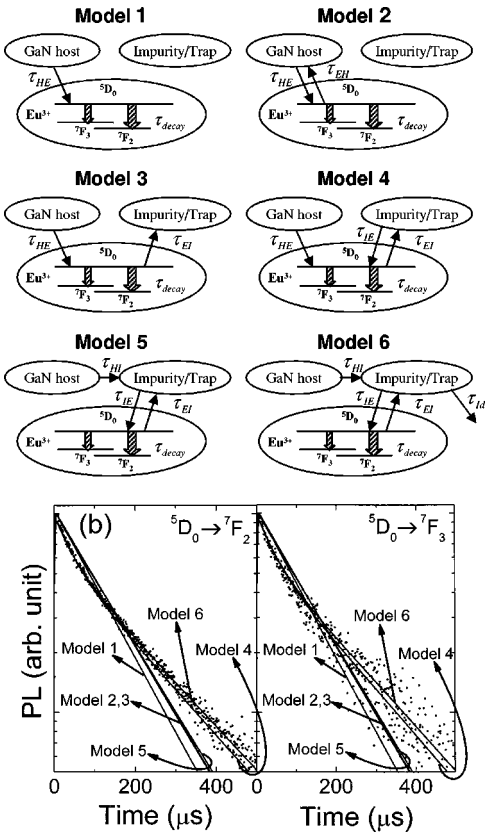


FIG. 5. (a) A schematic diagram of the various rate equation models considered in the text. (b) The TRPL data for both transitions at 303 K, overlaid by the best-fit results from each rate equation model. High temperature data was the most complex and therefore most useful in ascertaining the appropriateness of the various models.

Because both transitions share the common excited state $^5D_0$, the radiative decay rate for each transition could not be ascertained experimentally. Instead, a single decay rate from the $^5D_0$ state to the $^7F_J$ manifold $\tau_{\text{decay}}$ was obtained by the fit:

$$\frac{1}{\tau_{\text{decay}}} = \sum_i \frac{1}{\tau\left({}^5D_0 \rightarrow {}^7F_i\right)} \approx \frac{1}{\tau\left({}^5D_0 \rightarrow {}^7F_2\right)} + \frac{1}{\tau\left({}^5D_0 \rightarrow {}^7F_3\right)}. \quad (3)$$

Transition probabilities from $^5D_0$ to $^7F_J$ states other than $^7F_2$ and $^7F_3$ are tiny, so the radiative decay from $^5D_0$ is dominated by these two transitions and other radiative decay pathways may be ignored in the models. Global fits for the decay constants were obtained using a nonlinear least squares technique in which the $\chi^2$ merit function is minimized by adjusting the decay constants through the Levenberg–Marquardt scheme.[26] The TRPL data were fit by each model at each temperature, and the best fits for the room temperature data are given in Fig. 5(b).

The simplest model involves pump excitation of the GaN host, energy transfer to the $^5D_0$ state of the $Eu^{3+}$ ions, and decay involving the two radiative transitions studied [Model 1 of Fig. 5(a)]. The early time rising feature of the TRPL data is characterized by the host-to-$Eu^{3+}$ ($^5D_0$) energy transfer process with decay rate $\tau_{HE}$. Likewise, a single radiative and nonradiative population decay rate ($\tau_{\text{decay}}$) from the $^5D_0$ state to the $^7F_J$ states, including $^7F_2$ and $^7F_3$, provides the simplest simulation of the slowly decaying

TRPL data. Using this rudimentary Model 1, TRPL data at each temperature were fit and best values for $\tau_{HE}$ and $\tau_{\text{decay}}$ were obtained. However, as indicated in Fig. 5(b), the fit is poor and the model is inadequate because the decay is increasingly biexponential with increasing temperature. The data clearly demand a more complex model.

A candidate mechanism for the faster biexponential process ($\tau_{f2}, \tau_{f3}$) depopulating excited $Eu^{3+}$ ions is relaxation back to the host from the $^5D_0$ state of $Eu^{3+}$ ($\tau_{EH}$) (Model 2). This additional energy transfer process was also unable to simulate the data, especially in the higher temperature region. In fact, Model 2 provided fits to the data that were nearly identical in quality to Model 1. The reason for this is that the best-fit values for $\tau_{EH}$ in Model 2 were significantly slower than $\tau_{\text{decay}}$. Consequently, the predicted decay approximated single exponential decay characterized by $\tau_{\text{decay}}$, just as in Model 1. Thus, the back transfer process characterized by $\tau_{EH}$ can be omitted from the final model, but this does not imply that the process is unimportant. Instead, carriers returning to the host by the pathway they reached $^5D_0$ ($\tau_{EH}$) are quickly returned to $^5D_0$, because $\tau_{HE}$ is so fast, and therefore have no impact on the decay of $^5D_0$.

The results indicate that biexponential decay requires a reservoir with which $^5D_0$ can slowly exchange excitation in the presence of competing nonradiative decay pathways. Model 3 adds an energy transfer pathway to such a reservoir, likely an impurity or trap in the host, characterized by the decay constant $\tau_{EI}$ (Model 3). Surprisingly, this additional energy transfer process was no better able to simulate the data than Models 1 and 2. The best-fit values for $\tau_{EI}$ in Model 3 were significantly slower than $\tau_{\text{decay}}$, just as was seen for $\tau_{EH}$ in Model 2. This does not imply that transfer to the impurity/trap is unimportant. Rather, because there is no return mechanism from the impurity/trap to $^5D_0$, $\tau_{EI}$ cannot be faster than $\tau_{\text{decay}}$ or it would become the dominant (nonradiative) relaxation process, depopulating $^5D_0$ too quickly.

Two other return energy transfer processes must be considered: transfer from the impurity/trap to the host, and a direct return from the impurity/trap to the $^5D_0$ state. Either, or both, of these processes may be operative, and from a modeling perspective these two processes produce a nearly identical result. However, because the characteristic recombination time in the GaN host is a very rapid ~1 ns, the former process is unlikely to be effective in returning excitation from the reservoir to $^5D_0$. Therefore, Model 4 reflects the latter process, represented by the transfer rate $\tau_{IE}$ [Fig. 5(a)]. This model successfully fitted the data at each temperature, including room temperature as shown in Fig. 5(b). Inclusion of the former process yielded a fit of identical quality and, because of the speed of $\tau_{HE}$, only slightly different decay constants. Clearly, then, the model indicates that nonradiative energy transfer exchange between the $Eu^{3+}$ dopant and an impurity/trap reservoir is responsible for the faster decay process while maintaining a sizable $^5D_0$ excitation for the observed slow radiative decay.

For completeness, a fifth model was attempted that routed energy transfer between the host and the $Eu^{3+}$ through the impurity/trap state [Fig. 5(a)]. It is widely believed that capture of photoexcited carriers from a host to a RE dopant proceeds through an intermediate excitonic trap created by the dopant. The question that Model 5 addresses is whether that trap also acts as the impurity/trap reservoir for the $^5D_0$ state. The answer is no: Model 5 provided no better fit to the data than Models 2 and 3 [Fig. 5(b)], and for a similar reason. In order for Model 5 to transfer excitation from the GaN host to the $^5D_0$ state quickly enough, the decay constant $\tau_{IE}$ had to be very fast. Consequently, the impurity/trap state empties quickly and cannot be the long-lived trap state evident in the data. For this reason, Model 5 was deemed a poor representation of the energy transfer pathways.

However, the impurity/trap state could have an effectively slower decay if the return process $\tau_{EI}$ is also fast and a separate radiative and/or nonradiative decay channel is responsible for depleting the trap/impurity. A variant of Model 5 that also included a separate decay pathway from the impurity/trap state [Fig. 5(a)] was considered. This Model 6 provided fits that reproduced the data almost as well as Model 4 [Fig. 5(b)] but, for reasons that will be discussed below, is highly unlikely to reflect the true energy transfer pathways.

Therefore, Model 4 seems to be the best and simplest representation of the data and the underlying energy transfer mechanisms. The rate equations used in Model 4 are

$$\begin{aligned}
\frac{dN_{\text{host}}}{dt} &= g - \frac{1}{\tau_{HE}} N_{\text{host}}, \\
\frac{dN_{\text{trap}}}{dt} &= -\frac{1}{\tau_{IE}} N_{\text{trap}} + \frac{1}{\tau_{EI}} N_{\text{Eu}}, \\
\frac{dN_{\text{Eu}}}{dt} &= \frac{1}{\tau_{HE}} N_{\text{host}} + \frac{1}{\tau_{IE}} N_{\text{trap}} - \frac{1}{\tau_{\text{decay}}} N_{\text{Eu}} - \frac{1}{\tau_{EI}} N_{\text{Eu}},
\end{aligned} \tag{4}$$

where $g$ is the exciton generation rate, $N_{\text{host}}$ is the number of excitons in the host, $N_{\text{trap}}$ is the number of excitons in the impurity/trap state, and $N_{\text{Eu}}$ is the population of $Eu^{3+}$ ions in the excited $^5D_0$ state. Because pulsed excitation was used, $g$ was set to zero, and the effect of the pump was accommodated through the initial conditions: $N_{\text{host}}(t=0)=1$, $N_{\text{trap}}(t=0)=N_{\text{Eu}}(t=0)=0$.

A microscopic physical motivation for this model and the underlying rates and interpretation of the various energy transfer processes will be provided next.

## V. DISCUSSION

### A. Energy transfer from the host: $\tau_{HE}$

The long-range Coulomb attraction of photoexcited excitons to neutral/ionic donors is understood as the first step of energy transfer from the host to RE-dopants.[27] Evidence of this is seen in the broad cw emission spectrum below the GaN band gap, especially at low temperatures. An energy transfer process has been proposed, based on resonant Auger scattering, from the host to $Eu^{3+}$ ions in the $^5D_3$ state through the bound exciton recombination at a donorlike defect state below the conduction band minimum.[28–30] There are, in fact, two Auger mechanisms that may be operating. In one case, recombination of free excitons energetically excites $Eu^{3+}$ ions through resonant Auger scattering. In the other,

the free excitons are captured by Eu-related impurities/defects to form bound excitons that recombine to excite $4f$ core levels though resonant or nonresonant Auger scattering. Any energy defect in the Auger-mediated transfer is made up through phonon emission or absorption into a number of tightly spaced states in the $4f$ manifold, a process made critically important when it is realized that the GaN band gap changes by more than 70 meV over the temperature range of this experiment.

Both mechanisms involve energy transfer between the host and a number of $Eu^{3+}$ levels. Fourier transform infrared spectroscopy data suggest $Eu^{3+}$ doping provides concentration-dependent absorbing donor impurity levels, as much as 365 meV below the GaN conduction band, into which excitons are bound.[31,32] Nearly resonant with these impurity levels are a multitude of $Eu^{3+}$ $4f$ levels, the lowest of which is $^5D_3$, that form an almost continuous band and provide efficient energy transfer pathways for this Auger process to operate. These processes, whose expected temperature dependence[33] is not revealed within the measured temperature range, are not resolved in this experiment. The excited $4f$ electrons in the $^5D_J$ states relax sequentially until they reach $^5D_0$. However, no emission was observed from these intermediate states, so the detailed, level-specific energy transfer pathways could not be mapped in this work. Nevertheless, the collective effect of these energy transfer pathways was slow enough that the rate of net energy transfer from the host to the $^5D_0$ state of $Eu^{3+}$ could be measured and characterized. It is the cumulative effect of these processes that is modeled and represented by the decay rate $\tau_{HE}$.

Figure 6(a) shows that $\tau_{HE}$ is remarkably temperature insensitive at $\sim 0.4$ $\mu$s, and much slower than the $<10$ ns recombination rate of neutral-donor bound excitons in the GaN.[34] These apparently contradictory observations must be reconciled by positing that the Auger process occurs quickly, within the recombination lifetime of the excitons trapped at $Eu^{3+}$ sites. The subsequent relaxation within the $^5D_J$ manifolds, however, will be much slower,[25] and it is possible that a weak or nearly forbidden transition above $^5D_0$ is the bottleneck responsible for the temperature-insensitive rate. Therefore, the energy transfer process characterized by $\tau_{HE}$ represents the net effect of phonon-assisted Auger scattering of free or bound excitons to excite internal states within the $4f$ levels of $Eu^{3+}$. The rapidity of the process arises from the energetic overlap between the bound states and the $4f$ levels, with a high probability of back transfer,[30] while the temperature independence arises from a subsequent relaxation bottleneck prior to reaching $^5D_0$.

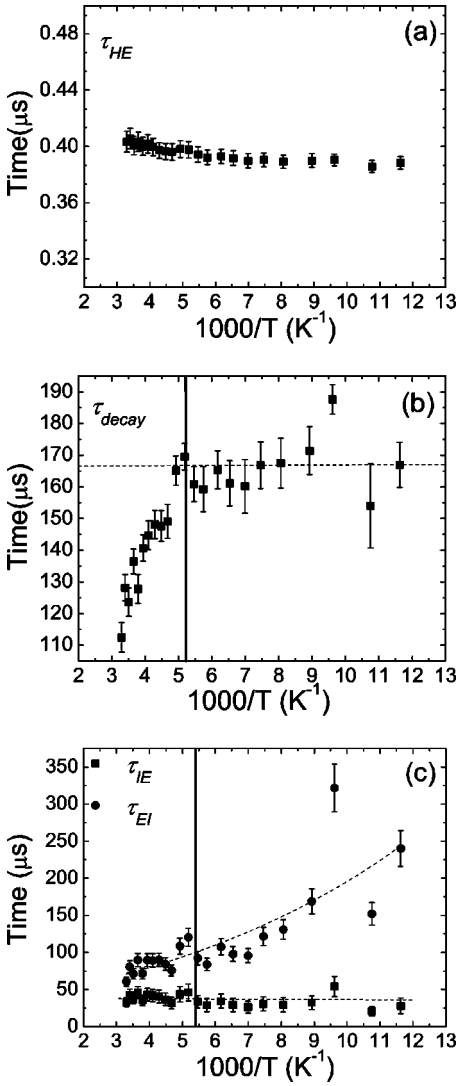


FIG. 6. The decay constants extracted from the data using Model 4, as a function of temperature. (a) The energy transfer decay constants from the GaN host to the $^5D_0$ state of the $Eu^{3+}$ ions ($\tau_{HE}$). (b) The total decay constants of the $^5D_0$ state $\tau_{\text{decay}}$. The low temperature radiative decay constant of 166 $\mu$s for the $^5D_0$ state is indicated by the dashed line. Above 180 K (left of the vertical line), the effects of an additional nonradiative process can be clearly seen. (c) The forward energy transfer decay constant from the $Eu^{3+}$ ions in the $^5D_0$ state to impurity/trap reservoir ($\tau_{EI}$) and the back transfer decay constant ($\tau_{IE}$).

### B. Decay from the $^5D_0$ state: $\tau_{\text{decay}}$

The biexponential fits of the $^5D_0 \rightarrow {}^7F_2$ and the $^5D_0 \rightarrow {}^7F_3$ transitions revealed a characteristic decay constant $\tau_{si}$ between 200 and 260 $\mu$s [Fig. 3(a)]. Because the frequency deviation from ionic vapor values is small and the linewidths are comparably narrow, these transitions are almost purely atomic and radiative in nature. This observation is borne out below 180 K, from which it could be assumed that the radiative relaxation decay constant for spontaneous emission from $^5D_0$ is $\tau_{s2} = \tau_{s3} \approx 250$ $\mu$s. However, notice that even at low temperatures these decay constants are not temperature-independent. By contrast, the values for $\tau_{\text{decay}}$ obtained from Model 4 below 180 K are a temperature independent 166 $\mu$s [Fig. 6(b)]. Thus, $\tau_{\text{decay}}$ represents the cumulative radiative emission rate from the $^5D_0$ state, and the difference between $\tau_{\text{decay}}$ and the $\tau_{si}$'s is now seen to be the increasingly important role played by slow, temperature-dependent energy transfer from $^5D_0$ to the impurity/trap state ($\tau_{EI}$). Following Eq. (3), radiative decay below 180 K almost exclusively involves $^5D_0 \rightarrow {}^7F_2$ and $^5D_0 \rightarrow {}^7F_3$. Although the TRPL data do not reveal the specific rates of these two transitions, the factor of 10 ratio of the CWPL intensities and the almost complete absence of emission from any other transition in-

volving $^5D_0$ suggests that the two decay constants may be estimated as $\tau_{7F2}=(11/10)\tau_{\text{decay}}=184\,\mu\text{s}$ and $\tau_{7F3}=(11/1)\tau_{\text{decay}}=1.84\,\text{ms}$.

Of course, $\tau_{\text{decay}}$ represents the total depopulation rate of $^5D_0$, both radiative and nonradiative. Above 180 K, Model 4 indicates a decrease of $\tau_{\text{decay}}$ with temperature [Fig. 6(b)], suggesting the onset of another relaxation pathway to depopulate $^5D_0$. The nature of this additional process is not known. However, several clues can be obtained from the data that constrain the possible mechanism. First, no new photoluminescence feature was observed to emerge above 180 K at any energies between 1.8 and 3.4 eV, so it can be assumed that this process is nonradiative. Subtracting out the radiative contribution to this total rate, the decay constant of this additional relaxation pathway is revealed as well as its temperature dependence. Second, this process is seen working in both transitions measured with identical decay constants, so the process must operate by depopulating the state $^5D_0$ or the manifold of states above it. Third, the fact that the rate of this process increases exponentially with temperature above 180 K suggests that this nonradiative process is a thermally activated process with an activation energy of 16 meV. By 300 K it already has a decay constant (344 $\mu$s) fully half the rate of the cumulative spontaneous emission decay constant (166 $\mu$s). Finally, because this same activation energy was observed operating in the fast biexponential decay feature, it must be assumed that the two processes are related, perhaps by a common energy level 16 meV above the $^5D_0$ state of $Eu^{3+}$. Since this faster feature is characterized in the rate equations model by the energy transfer between the $Eu^{3+}$ and impurity/trap states, it is now necessary to investigate that process further.

### C. Energy transfer with the impurity/trap state: $\tau_{EI}$ and $\tau_{IE}$

For energy transfer to the impurity/trap states ($\tau_{EI}$) and for back transfer from these states to $^5D_0$ ($\tau_{IE}$), the two decay constants were first fit as independently adjustable parameters. The result is plotted in Fig. 6(c). The back transfer process from the impurity/trap reservoir was fairly independent of temperature ($\tau_{IE}=36\,\mu\text{s}$) while the forward transfer to the reservoir accelerated rapidly with increasing temperature ($\tau_{EI}=250-70\,\mu\text{s}$). It was found, not surprisingly, that the two processes were correlated by a detailed balance relationship, namely,

$$\frac{1}{\tau_{EI}}=\frac{1}{\tau_{IE}}\exp\left(-\frac{\Delta E}{kT}\right). \tag{5}$$

The value of the energy difference $\Delta E$ obtained from a fit of the $\tau_{EI}$ versus temperature [dashed lines in Fig. 6(c)] is 14.7 $\pm$0.8 meV. Note that this is the fourth independent indication from the data that an impurity/trap state has an activation energy of approximately 16 meV above $^5D_0$.

There is ample precedent for the important role played by impurity/trap states in the energy relaxation of rare earth-doped semiconductors.[27] It must be emphasized here that the impurity/trap reservoir plays a very different role than the donor state formed by the $Eu^{3+}$ dopant. This is most clearly recognized by noting that $\tau_{IE}$ is almost 100 times slower than $\tau_{HE}$. (Indeed, this is the reason that Model 5 failed.) Nevertheless, both processes share many common characteristics. Both probably represent a composite of several relaxation pathways. As originally suggested by Taguchi *et al.* to explain thermal quenching of the luminescence from Yb-doped InP, the back transfer process $\tau_{IE}$ probably involves nonresonant Auger scattering assisted by multiphonon emission/absorption.[35] Likewise, the return from the impurity/trap reservoir to $^5D_0$ ($\tau_{IE}$) may proceed through a number of pathways, perhaps including the multistep process characterized by $\tau_{HE}$. However, because $\tau_{IE}$ is much longer than the recombination time in the GaN host, it is clear that the impurity/trap state is well isolated from the host and the $Eu^{3+}$ dopants. Further proof of this isolation is the fact that $\Delta E$ does not change with temperature even though the GaN band gap changes by more than 70 meV over the measured temperature range. Thus, the primary relaxation mechanism transfers excitation directly back to the $Eu^{3+}$ dopants. Because both $\tau_{HE}$ and $\tau_{IE}$ are insensitive to temperature, temperature-independent rate-limiting transitions in the relaxation pathways are common in both processes.

The remaining question is whether there is a separate decay mechanism within the trap/impurity state that is responsible for the accelerated $\tau_{\text{decay}}$ observed above 180 K [Fig. 6(b)]. Model 6 was one attempt to consider this by including an additional decay constant $\tau_{Id}$ from the trap/impurity state to the ground state. A variant of Model 4 with a $\tau_{Id}$ process was also attempted. Although both models were able to reproduce the data, the resulting fits were unstable and the decay constants were unacceptably sensitive to the values of the other fitted parameters, even when some of them were fixed in the fit. This does not disprove the existence of a separate impurity/trap decay mechanism; however, it does indicate that it is not primarily responsible for the accelerated $\tau_{\text{decay}}$ observed above 180 K. Instead, the accelerated $\tau_{\text{decay}}$ most likely arises from an additional nonradiative decay process depopulating $^5D_0$.

### D. Implications of the models

What exactly the impurity/trap reservoir is or why the transfer to $^5D_0$ is so slow is unresolved. Nevertheless, several observations from the data constrain the answer. If one assumes a homogeneously and uniformly doped host, the impurity/trap reservoir must either be an internal state of the $Eu^{3+}$ or related to a vacancy or inadvertent dopant in the host connected to $^5D_0$ through an Auger or multiphonon process. Of course, no sample is isotropically doped, and other possibilities arise. The most straightforward of these assumes a Poissonian distribution of $Eu^{3+}$ dopant placement in which some dopants are quite isolated and exhibit atomic like relaxation, while other dopants aggregate. This may be exacerbated by the fact that not all dopants will be found at $C_{3v}$ substitutional sites. As shown by Inokuti and Hirayama[20] multipolar interactions among dopants increase dramatically in effectiveness as the interdopant spacing decreases. Collective and cooperative interactions among the clustered dopants may be partially responsible for the nonradiative relaxation pathways whose effectiveness increases with increasing

temperature. As a further complication, the host itself is unlikely to be isotropic. GaN is notorious for threading and screw dislocations and N-vacancies, all of which could play a role as either a dopant nucleation site or as an impurity/trap reservoir. Although such imperfections have not prevented efficient luminescence from III–N based heterostructures and nanostructures, they may play a more important role in the nonradiative relaxation of RE-dopants given their sensitivity to very local conditions. Given that the measured TRPL data samples heterogeneous $Eu^{3+}$ dopant distributions and interactions in the anisotropic GaN host, a complete reconciliation of these effects will require analysis beyond the scope of this work.

For the purposes of this work, however, a critical point must be made. It is common in the analysis of decay in RE-doped materials to fit a simple or modified exponential or biexponential function to the data in order to extract decay constants.[21,22] Often these decay constants are interpreted by a microscopic theory that assumes a certain degree of homogeneity and sample purity that is rarely found, especially in the GaN system. The insights provided by the analysis above arise not from the application of an approximate theory to the data, but by using rate equation models to extract information as the data reveals it. In particular, it is quite inappropriate to equate the radiative decay of the $^5D_0$ transition with the slow feature of the biexponential fit. The data clearly indicate the role of nonradiative pathways that would not have been predicted *ab initio*, and may indeed arise from material imperfections. Nevertheless, they are of critical importance in order to develop optimal materials. Only when these nonradiative pathways are considered can the true spontaneous emission decay constant $\tau_{\text{decay}}$ of the $^5D_0$ state be ascertained.

## VI. CONCLUSION

In summary, temperature-dependent energy transfer mechanisms of Eu-doped GaN were investigated using time-resolved photoluminescence measurements of the $^5D_0 \rightarrow {}^7F_2$ and $^5D_0 \rightarrow {}^7F_3$ transitions. The luminescence decay was analyzed by numerically integrated rate equation models, and the decay constants of the energy transfer processes were extracted by using a nonlinear least-squares technique to fit the model predictions to the data. The GaN host was photoexcited by 300 nm, $<$200 fs optical pulses, and the energy transfer from the host to the $^5D_0$ state of the $Eu^{3+}$ ions was deduced to proceed through free and bound exciton trapped states with a temperature independent decay constant of 0.4 $\mu$s. The radiative decay rate of the $^5D_0$ state was measured to be 166 $\mu$s. A nonradiative relaxation pathway connecting the $^5D_0$ state to an impurity or trap was observed to operate with an energy defect of 16 meV. Various rate equation models were used to rule out a number of plausible energy transfer pathways and to reveal the inappropriateness of ascribing the slower component of biexponential decay to the radiative lifetime of the $^5D_0$ state.

## ACKNOWLEDGMENTS

C.-W. Lee would like to thank Michael D. Stenner for helpful discussions. Work at Duke University and at the University of Cincinnati was supported by Army Research Office Grants Nos. DAAG55-98-D-0002 and DAAD19-99-1-0348, respectively.

[1] A. J. Steckl and J. M. Zavada, MRS Bull. **24**, 33 (1999).
[2] D. S. Lee, J. Heikenfeld, R. Birkhahn, B. K. Lee, and A. J. Steckl, Appl. Phys. Lett. **76**, 1525 (2000).
[3] J. Heikenfeld, M. Garter, D. S. Lee, R. Birkhahn, and A. J. Steckl, Appl. Phys. Lett. **75**, 1189 (1999).
[4] W. M. Jadwisienczak, H. J. Lozykowski, A. Xu, and B. Patel, J. Electron. Mater. **31**, 776 (2002).
[5] A. J. Steckl, J. C. Heikenfeld, D. S. Lee, M. J. Garter, C. C. Baker, Y. Wang, and R. Jones, IEEE J. Sel. Top. Quantum Electron. **8**, 749 (2002).
[6] H. Bang, S. Morishima, Z. Li, K. Akimoto, M. Nomura, and E. Yagi, J. Cryst. Growth **237–239**, 1027 (2002).
[7] T. Maruyama, S. Morishima, H. Bang, K. Akimoto, and Y. Nanishi, J. Cryst. Growth **237–239**, 1167 (2002).
[8] P. H. Citrin, P. A. Northrup, R. Birkhahn, and A. J. Steckl, Appl. Phys. Lett. **76**, 2865 (2000).
[9] U. Wahl, A. Vantomme, G. Langouche, J. P. Araújo, L. Peralta, J. G. Correia, and the ISOLDE Collaboration, J. Appl. Phys. **88**, 1319 (2000).
[10] B. R. Judd, Phys. Rev. **127**, 750 (1962).
[11] G. S. Ofelt, J. Chem. Phys. **37**, 511 (1962).
[12] M. J. Weber, T. E. Varitimos, and B. H. Matsinger, Phys. Rev. B **8**, 47 (1973).
[13] D. Dragoman and M. Dragoman, *Optical Characterization of Solids* (Springer, New York, 2002).
[14] S. Hüfner, *Optical Spectra of Transparent Rare Earth Compounds* (Academic, New York, 1978).
[15] Ei Ei Nyein, U. Hömmerich, J. Heikenfeld, D. S. Lee, A. J. Steckl, and J. M. Zavada, Appl. Phys. Lett. **82**, 1655 (2003).
[16] H. J. Lozykowski, W. M. Jadwisienczak, J. Han, and I. G. Brown, Appl. Phys. Lett. **77**, 767 (2000).
[17] C. Brecher, H. Samelson, A. Lempicki, R. Riley, and T. Peters, Phys. Rev. **155**, 178 (1967).
[18] G. H. Dicke, *Spectra and Energy Levels of Rare Earth Ions in Crystals* (Wiley, New York, 1968).
[19] T. Monteiro, C. Boemare, M. J. Soares, R. A. Sá Ferreira, L. D. Carlos, K. Lorenz, R. Vianden, and E. Alves, Physica B **308–310**, 22 (2001).
[20] M. Inokuti and F. Hirayama, J. Chem. Phys. **43**, 1978 (1965).
[21] J. Hegarty, D. L. Huber, and W. M. Yen, Phys. Rev. B **25**, 5638 (1982).
[22] H. J. Lozykowski, W. M. Jadwisienczak, and I. G. Brown, J. Appl. Phys. **88**, 210 (2000).
[23] O. B. Gusev, M. S. Bresler, P. E. Pak, I. N. Yassievich, M. Forcales, N. Q. Vinh, and T. Gregorkiewicz, Phys. Rev. B **64**, 075302 (2001).
[24] S. F. Chichibu, Y. Kawakami, and T. Sota, in *Introduction to Nitride Semiconductor Blue Lasers and Light Emitting Diodes*, edited by S. Nakamura and S. F. Chichibu (Taylor and Francis, New York, 2000), Chap. 5, pp. 153–270.
[25] D. R. Tallant, C. H. Seager, and R. L. Simpson, Mater. Res. Soc. Symp. Proc. **621**, Q2.5.1 (2000).
[26] W. H. Press, B. P. Flannery, S. A. Tuekolsky, and W. T. Vetterling, *Numerical Recipes in C: The Art of Scientific Computing* (Cambridge University Press, Cambridge, 1988).
[27] M. Forcales, M. Klik, N. Q. Vinh, I. V. Bradley, J.-P. R. Wells, and T. Gregorkiewicz, J. Lumin. **94–95**, 243 (2001).
[28] J. Palm, F. Gan, B. Zheng, J. Michel, and L. C. Kimerling, Phys. Rev. B **54**, 17603 (1996).
[29] F. Priolo, G. Franzò, S. Coffa, and A. Carnera, Phys. Rev. B **57**, 4443 (1998).
[30] M. Godlewski, A. J. Zakrzewski, and V. Yu. Ivanov, J. Alloys Compd. **300–301**, 23 (2000).
[31] H. Bang, S. Morishima, Z. Li, K. Akimoto, M. Nomura, and E. Yagi, Phys. Status Solidi B **228**, 319 (2001).
[32] Z. Li, H. Bang, G. Piao, J. Sawahata, and K. Akimoto, J. Cryst. Growth **240**, 382 (2002).
[33] I. N. Yassievich and L. C. Kimerling, Semicond. Sci. Technol. **8**, 718 (1993).
[34] J. S. Im, A. Moritz, F. Steuber, V. Härle, F. Scholz, and A. Hangleiter, Appl. Phys. Lett. **70**, 631 (1997).
[35] A. Taguchi, K. Takahei, and Y. Horikoshi, J. Appl. Phys. **76**, 7288 (1994).